Scalability Analysis of LoRa Network for SNR-Based SF Allocation Scheme

Deepak Saluja, Rohit Singh, Lalit Kumar Baghel, and Suman Kumar

***Abstract*—Over the past few years, we have witnessed an explosive increase in the number of long range wide area network (LoRaWAN) devices, primarily because LoRaWAN offers attractive features such as long-range, low-power, and low-cost communications. However, the scalability of LoRaWAN is a major concern, which in particular depends on spreading factor (SF) allocation schemes. Primarily, SFs are assigned based on distance from the gateway, using equal-interval-based (EIB) and equal-area-based (EAB) SF allocation schemes. In this article, we have proposed an SNR-based SF allocation scheme to improve the scalability of LoRaWAN. We have introduced two different algorithms for the proposed scheme. Using stochastic-geometry, an analytical framework is developed for both the algorithms, and the expressions are derived for the packet success probability (PSP) under the co-SF interference scenario. In addition, the impact of an inter-SF interference on the PSP performance is analyzed by simulations. The proposed algorithms are compared with the EIB and EAB SF allocation schemes, and it is shown that the proposed algorithms perform better than the other two schemes. We have also analyzed the impact of end device density, packet size, and cell-radius on the LoRaWAN scalability. Moreover, we have performed real-time experiments to prove the applicability of the presented work in practical scenarios.**

***Index Terms*—LoRa network, long range wide area network (LoRaWAN), scalability, spreading factor (SF) allocation, stochastic geometry.**

I. Introduction

LOW-POWER wide-area network (LPWAN) technologies have emerged as promising technologies for the internet-of-things (IoT) due to their ability to support low-power, and long-distance communications [1], [2]. The popular LPWAN technologies are LoRa, sigfox [3], and narrow band-IoT [4]. An introduction and comparison of these LPWAN technologies are presented in [1] and [5]. Among all these LPWAN technologies, LoRa has attracted more attraction due to its open standards that allow an individual to build an autonomous network at lower cost [6]. In addition, the LoRa network operates in the unlicensed sub-GHz band and uses the chirp spread spectrum (CSS) modulation [7], [8]. The chirp signal changes its frequency linearly with time, which makes the LoRa network resistant to interference. The capabilities and limitations of the LoRa network are presented in [6] and [9].

The implementation of LoRaWAN[1] in various sectors, including smart metering, home, industry, agriculture, office, and city, have led to rapid growth in the number of LoRa devices [10], [11]. With the rapid growth in LoRa devices, the LoRaWAN scalability has become a major concern [9]. In general, the scalability of LoRaWAN is affected by random-access protocol: LoRaWAN is based on the unslotted ALOHA protocol, where packets access shared channels randomly, hence affecting the scalability; and cospreading factor (co-SF) interference: the transmission of packets at the same SF and frequency leads to interference, known as co-SF interference [12]. The packets accessing the shared channel over the same SF leads to the collision of packets, which further affects the scalability of the LoRaWAN [9], [13]. Therefore, the scalability of LoRaWAN depends greatly on the SF allocation schemes [14], [15].

In the literature, the scalability of LoRaWAN is mainly analyzed for distance-based SF allocation schemes. In distance-based SF allocation schemes, end devices (EDs) are assigned SF based on their distance from the gateway. Essentially, distance-based SF allocation strategies consider two types of SF allocation schemes: equal-interval-based (EIB) and equal-area-based (EAB). In both schemes, the total network area are divided into K concentric circles, where each annulus gets an equal width in the EIB scheme, while each annulus gets an equal area in the EAB scheme. However, in a realistic environment, it is possible that the ED near the gateway receives a packet with a low signal-to-noise-ratio (SNR), while the ED away from the gateway receives a packet with a high SNR. Therefore, these SF allocation schemes are not efficient enough from the scalability perspective. In this article, we proposed an SNR-based SF allocation scheme to improve the scalability of LoRaWAN.

Manuscript received July 19, 2020; revised October 31, 2020 and November 29, 2020; accepted November 30, 2020. Date of publication December 7, 2020; date of current version June 30, 2021. This work was supported by the Department of Science and Technology, Government of India, for the Technology Innovation Hub at the Indian Institute of Technology Ropar in the framework of National Mission on Interdisciplinary Cyber-Physical Systems (NM—ICPS). Paper no. TII-20-3469. *(Corresponding author: Deepak Saluja.)*

The authors are with the Department of Electrical Engineering, Indian Institute of Technology Ropar, Rupnagar 140 001, India (e-mail: 2016eez0009@iitrpr.ac.in; 2017eez0007@iitrpr.ac.in; lalit.19eez0026@iitrpr.ac.in; suman@iitrpr.ac.in).

Color versions of one or more figures in this article are available at https://doi.org/10.1109/TII.2020.3042833.

Digital Object Identifier 10.1109/TII.2020.3042833

[1]LoRaWAN is a medium access control layer protocol designed to handle long-range communication between EDs and gateways at low power.

II. Related Works and Contributions

The scalability of LoRaWAN for different SF allocation schemes has been analyzed in [14]–[17]. In particular, the authors in [14] analyzed the scalability of the LoRaWAN for the EIB scheme. In [15], the authors analyzed the scalability using network simulator-3 for three SF allocation schemes; first, random SF allocation; second, fixed SF allocation, which assigned the same SF to each ED; and third, based on the packet error ratio. Similarly, the authors in [16] considered three different SF allocation schemes based on the distance between gateway and EDs. In [17], the authors compared the EIB, EAB, and path-loss based SF allocation schemes. In a different line of research, the reliability of the LoRaWAN is analyzed in [18] and [19], where they considered a fixed SF allocation.

In [20], the authors have considered the SF allocation schemes based on received-signal-strength-indicator and time-on-air parameters. The work in [21] considered the optimization of distance parameters[2] to improve the scalability of the LoRa network. Apart from the scalability analysis, in [22], the authors analyzed the throughput of the LoRaWAN based on distance-based SF allocation scheme. Recently, in [23], the authors proposed distance-based SF allocation scheme based on the Fibonacci series, arithmetic series, square numbers, and wythoff array. In these schemes, the area assigned to each SF varies according to their respective functions.

From the existing literature, two major challenges have been identified; first, in a realistic propagation environment (where small scale fading is prevalent), the existing SF allocation schemes, i.e., EIB and EAB schemes, are not efficient enough since these schemes do not consider the impact of channel fading; second, the scalability offered by existing SF allocation schemes is limited. Therefore, in this article, we address these challenges by proposing a novel SNR-based SF allocation scheme that allocates SF based on considering the impact of channel fading along with distance. To the best of our knowledge, such an SF allocation scheme and its study have not yet been presented in the literature to date.

A. Contributions

In this article, we have proposed a novel SF allocation scheme to improve the scalability of the LoRa network. The key contributions of the article are as follows.

1) A novel SF allocation scheme based on the SNR of the received packet is proposed. In particular, we developed two heuristic algorithms for the proposed SF allocation scheme. Using stochastic-geometry, an analytical framework is developed for both the algorithms, and the expressions are derived for the packet success probability (PSP) under the co-SF interference scenario.
2) The impact of an inter-SF interference on PSP performance is also analyzed. Furthermore, the scalability of both algorithms is compared with the state-of-art SF allocation schemes, i.e., EIB and EAB schemes. It has been shown that the proposed algorithms provide better scalability as compared to the EIB and EAB SF allocation schemes.
3) To prove the applicability of the presented work in practical scenarios, we have performed real-time experiments and have shown SNR variations with distance. Based on our proposal, we have highlighted and incorporated the required changes in the blocks of the LoRaWAN system. Furthermore, we have listed some real-life applications that can be solved from the presented work.

[2]Note that the optimization of the distance parameter is corresponding to the optimization of the area assigned to each SF.

TABLE I
LoRa Modulation Parameters for 10 Bytes Packet

SF	$\hat{s}$	Data rate (kbps)	Packet duration $t_{\hat{s}}$ (sec)	SNR threshold $\Delta_{\hat{s}}$ (dB)	Range $r_{\hat{s}}$
7	1	5.47	0.036	-6	$[r_0, r_1]$
8	2	3.13	0.062	-9	$[r_1, r_2]$
9	3	1.76	0.124	-12	$[r_2, r_3]$
10	4	0.98	0.248	-15	$[r_3, r_4]$
11	5	0.54	0.414	-17.5	$[r_4, r_5]$
12	6	0.29	0.827	-20	$[r_5, r_6]$

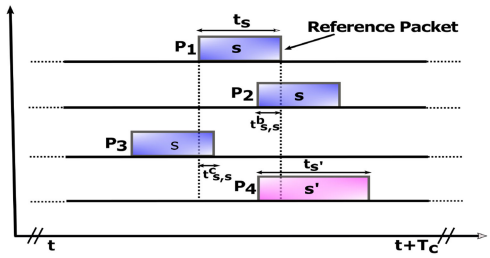

Fig. 1. Illustration of packet collision in LoRaWAN.

III. System Model

We considered an uplink LoRa network, consisting of N EDs and a gateway, distributed in a circular disc of radius R. The EDs are distributed according to homogeneous Poisson point process (PPP) ξ with density $\rho = \frac{\bar{N}}{\pi R^2}$, where $\bar{N}$ defines the mean of Poisson random variable N. While the gateway is assumed to be located at the center (origin) of the disc. The channel between gateway and EDs is assumed to be Rayleigh faded. Each ED is assigned an index $\hat{s}$ from the set $\mathbb{S} = \{1, 2, \ldots, S\}$. Where the parameter S defines the cardinality of the set of available SFs, i.e., $S = |\mathbb{S}|$. Note that these indices are related to SF, as shown in Table I. It is assumed that SNR is known at the gateway [21], [24].

The packet transmission in LoRaWAN is based on the unslotted ALOHA protocol; consequently, there is a high probability of packet collision. The packet collision in LoRaWAN is better illustrated in Fig. 1. Here, we have considered four EDs. Each ED transmits its packet randomly within the contention period T_c using ALOHA protocol. The packet P_1 with SF s is considered as a reference packet. Since the packets (P_2, and P_3) also transmit with SF s, they act as an interference sources. The probability density function (pdf) of collision overlap time under co-SF

interference is defined as [21],

$$f_{t_{\hat{s},\hat{s}}}(t) = \left(1 - \frac{t_{\hat{s}}(2T_c - t_{\hat{s}})}{T_c^2}\right)\delta(t) + \frac{2t}{T_c^2} + \frac{2}{T_c}\left(1 - \frac{t_{\hat{s}}}{T_c}\right) \quad (1)$$

where $\delta(.)$ is the Dirac delta function, $t_{\hat{s}}$ denotes the packet duration of SF $\hat{s}$, and $t_{\hat{s},\hat{s}}$ denotes the collision overlap time under co-SF interference scenario. The first term on the right-hand-side of (1) signifies the pdf of the case where there is no collision of packets. While the second term signifies the pdf of the packet collision (overlapped) case (i.e., the packets are either completely overlapped or partially overlapped).

The CSS modulation parameters of the LoRa packet for SF $\hat{s}$, where $\hat{s} = \{1, \ldots, 6\}$, are provided in Table I. Note that the values in Table I are shown for 125 kHz bandwidth and 10 b of packet size. The signal-to-interference-ratio (SIR) of a typical ED with SF $\hat{s}$, located at a distance r meters from the gateway under co-SF interference, is given by

$$\eta_{\hat{s}}(r) = \frac{A_0\, g r^{-\alpha}}{I_{\hat{s},\hat{s}}}, \qquad I_{\hat{s},\hat{s}} = \sum_{\hat{s} \in \phi_{\hat{s}}/S_0} A_0 g_{\hat{s}} r_{\hat{s}}^{-\alpha} \frac{t_{\hat{s},\hat{s}}}{t_{\hat{s}}} \quad (2)$$

where $A_0 = (\frac{c}{4\pi f_c})^2$, which comes from friis transmission equation with carrier frequency f_c and velocity of light c. Here, r and r_j denote the distance from the gateway to typical ED and jth interfering ED, respectively, while g and g_j denote their corresponding channel fading power. These fading powers are assumed to be independent and identically exponentially distributed with a unit mean i.e., $g \sim \exp(1)$ and $g_{\hat{s}} \sim \exp(1)$. $\phi_{\hat{s}}/S_0$ denotes the set of all EDs operating at SF s, except the typical ED (S_0). Note that factor $\frac{t_{\hat{s},\hat{s}}}{t_s}$ is for normalizing the interference power [21].

IV. Development of SNR-Based SF Allocation Scheme

In the LoRa network, the analysis is typically carried out in two steps. The primary step is to allocate SFs to EDs based on the considered SF allocation scheme. Then, the analysis is performed over the considered SF allocation scheme. This section gives the motivation for the proposed SNR-based SF allocation scheme and focuses on its development. While its PSP analysis is provided in the next section.

In the existing SF allocation schemes viz., EIB, and EAB schemes, EDs are assigned SF based on their distance from the gateway. However, in a realistic environment, it is possible that the ED near the gateway receives a packet with a low SNR, while the ED away from the gateway receives a packet with a high SNR. Since these schemes do not consider the impact of channel fading, they are not efficient enough from the scalability perspective. Therefore, we proposed the SNR-based SF allocation scheme. SNR-based SF allocation scheme assigns SFs to EDs based on the SNR (i.e., it considers the impact of both the channel fading and distance in SF allocation) of the received packet. The SNR $\Upsilon(r)$ of a typical ED located at a distance r meters from the gateway is given by

$$\Upsilon(r) = \frac{P A_0\, g r^{-\alpha}}{\sigma^2} \quad (3)$$

where P denotes the transmit power of ED, while σ^2 denotes the noise power. The development of SNR-based SF allocation scheme is based on (3). Here, (3) signifies that the SNR of a typical ED located at a fixed distance from the gateway varies with small-scale fading.

A visual comparison of SNR-based SF allocation with EIB and EAB is shown in Fig. 2, where we assume $N = 2700$ in a circular disc of $R = 20$ km. It can be seen that, for EIB and EAB SF allocation schemes, there are fixed boundaries of annulus for each SF. Whereas for the proposed SF allocation scheme, SFs are mixed in a circular disc, that is, there are no definite boundaries of annulus for each SF. This is because the SNR-based SF allocation scheme allocates SFs considering both the channel fading and distance. Therefore, it is possible that a higher SF is assigned to the ED near the gateway, while a lower SF is assigned to the ED away from the gateway. Based on the proposed SNR-based SF allocation scheme, we have developed two heuristic algorithms. A description of each algorithm, including their expressions for the PSP under the co-SF interference scenario, is given in next section.

V. Proposed Algorithms

Proposed Algorithm 1 (PA1): PA1 assigns SF based on target SNR ($\Delta_{\hat{s}}$) of the SF $\hat{s}$. The number of EDs experiencing SNR greater than Δ_1 (which is -6 dB, given in Table I) are assigned SF7. While the number of EDs experiencing SNR between Δ_j and Δ_{j-1} (i.e., $\Delta_j < \gamma < \Delta_{j-1}$) for $j = \{2, 3, \ldots, 6\}$ are assigned SF corresponding to j. Note that the lower SF has a relatively low packet collision probability and provides a high data-rate. However, it possesses relatively low receiver sensitivity compared to higher SF. Keeping these facts in mind, PA1 assigns SFs based on target SNR, starting with lower SF (SF7). In the next section, we will obtain the expression of the PSP for PA1.

A. PSP: PA1

PSP defines the average fraction of EDs that can successfully communicate with the gateway. For PA1, the PSP contributed by EDs that are assigned SF7 can be defined as

$$\begin{aligned} \text{PSP}_{PA1}(r, \delta_1) &= \mathbb{P}\left[\{\eta_1(r) > \delta_1\} \bigcap \{\Upsilon(r) > \Delta_1\}\right] \\ &\geq \mathbb{P}[\eta_1(r) > \delta_1]\mathbb{P}[\Upsilon(r) > \Delta_1]. \end{aligned} \quad (4)$$

The inequality in (4) holds because the conditional probability is greater than the unconditional probability. Note that the inequality is tight for an interference-limited scenario [25]. The PSP contributed by EDs assigned with SF j, where $j \in \{2, \ldots, S\}$ can be defined as

$$\begin{aligned} \text{PSP}_{PA1}(r, \delta_j) &= \mathbb{P}\left[\{\eta_j(r) > \delta_j\} \bigcap \{\Delta_j < \Upsilon(r) < \Delta_{j-1}\}\right] \\ &\geq \mathbb{P}\left[\eta_j(r) > \delta_j\right] \mathbb{P}\left[\Delta_j < \Upsilon(r) < \Delta_{j-1}\right] \\ &\qquad j = \{2, \ldots, S\}. \end{aligned} \quad (5)$$

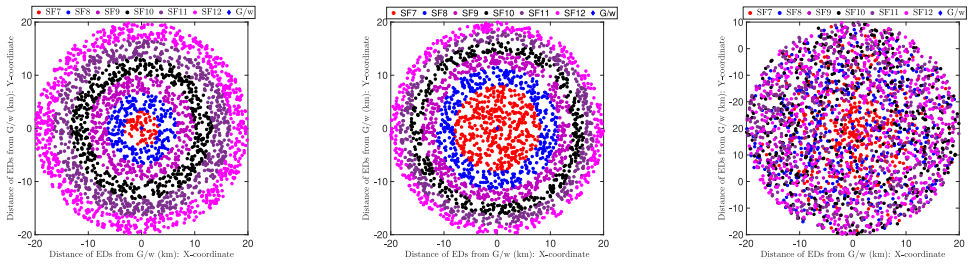

(a) (b) (c)

Fig. 2. SF allocation for $\bar{N} = 2700$ in a circular disk of $R = 20$ km for three different SF allocation schemes. Here, G/w stands for gateway. (a) EIB scheme. (b) EAB scheme. (c) SNR-based scheme.

Since $g \sim \exp(1)$, the second term in (4) can be calculated as

$$\mathbb{P}[\Upsilon(r) > \Delta_1] = P_{\gamma_1} = \exp\left\{-\frac{\Delta_1 \sigma^2 r^\alpha}{PA_0}\right\} \tag{6}$$

which defines the average fraction of EDs that are having SNR greater than Δ_1. While the second term in (5) (let it be denoted by P_{Υ_j}) can be expressed as below [given by (7)], where its proof follows from the assumption that $g \sim \exp(1)$:

$$\begin{aligned} P_{\Upsilon_j} &= \mathbb{P}\left[\Delta_j < \Upsilon(r) < \Delta_{j-1}\right] \\ &= \mathbb{P}[\Upsilon(r) > \Delta_j] - \mathbb{P}[\Upsilon(r) > \Delta_{j-1}] \\ &= \exp\left(-\frac{\Delta_j \sigma^2 r^\alpha}{PA_0}\right) - \exp\left(-\frac{\Delta_{j-1}\sigma^2 r^\alpha}{PA_0}\right), \\ j &= \{2, \ldots, S\}. \end{aligned} \tag{7}$$

Now we obtain the expression for the first term in (4) and (5), which can be expressed together in a more general form as

$$\begin{aligned} \mathbb{P}[\eta_{\hat{s}}(r) > \delta_{\hat{s}}] &= \mathbb{E}_{I_{\hat{s},\hat{s}}}\left[\mathbb{P}\left[\frac{A_0\, g r^{-\alpha}}{I_{\hat{s},\hat{s}}} > \delta_{\hat{s}}\right]\right] \\ &\overset{(a)}{=} \mathbb{E}_{I_{\hat{s},\hat{s}}}\left[\exp\left(\frac{-\delta_{\hat{s}} I_{\hat{s},\hat{s}} r^\alpha}{A_0}\right)\right] \\ &\overset{(b)}{=} \mathcal{L}_{I_{\hat{s},\hat{s}}}\left(\frac{\delta_{\hat{s}} I_{\hat{s},\hat{s}} r^\alpha}{A_0}\right), \hat{s} = \{1, 2, \ldots, S\}. \end{aligned} \tag{8}$$

Note that, for $\hat{s} = 1$, (8) is corresponding to SF7 [i.e., the first term of (4)]. Here, (a) follows from $g \sim \exp(1)$ and (b) follows from the definition of Laplace transform, where $\mathcal{L}_{I_{\hat{s},\hat{s}}}(.)$ denotes the Laplace transform of $I_{\hat{s},\hat{s}}$. Assuming $s = \frac{\delta_{\hat{s}} r^\alpha}{A_0}$, the Laplace transform of $I_{\hat{s},\hat{s}}$ can be expanded as

$$\begin{aligned} \mathcal{L}_{I_{\hat{s},\hat{s}}}(s) &= \mathbb{E}[\exp(-sI_{\hat{s},\hat{s}})] \\ &= \mathbb{E}_{\phi_{\hat{s}}/S_0, g_{\hat{s}}, t_{\hat{s},\hat{s}}}\left[\exp\left(-s \sum_{\hat{s}\in\phi_{\hat{s}}/S_0} A_0 g_{\hat{s}} r_{\hat{s}}^{-\alpha} \frac{t_{\hat{s},\hat{s}}}{t_{\hat{s}}}\right)\right] \\ &= \mathbb{E}_{\phi_{\hat{s}}/S_0, g_{\hat{s}}, t_{\hat{s},\hat{s}}}\left[\prod_{\hat{s}\in\phi_{\hat{s}}/S_0} \exp\left(-s g_{\hat{s}} r_{\hat{s}}^{-\alpha} \frac{t_{\hat{s},\hat{s}}}{t_{\hat{s}}}\right)\right]. \end{aligned} \tag{9}$$

Since $g_{\hat{s}} \sim \exp(1)$, using moment generation function, (9) can be expressed as

$$\begin{aligned} \mathcal{L}_{I_{\hat{s},\hat{s}}}(s) &= \mathbb{E}_{\phi_{\hat{s}}/S_0, t_{\hat{s},\hat{s}}}\left[\prod_{\hat{s}\in\phi_{\hat{s}}/S_0} \frac{1}{1 + sA_0 r_{\hat{s}}^{-\alpha} \frac{t_{\hat{s},\hat{s}}}{t_{\hat{s}}}}\right] \\ &= \mathbb{E}_{\phi_{\hat{s}}/S_0}\left[\prod_{\hat{s}\in\phi_{\hat{s}}/S_0} \mathbb{E}_{t_{\hat{s},\hat{s}}}\left[\frac{1}{1 + sA_0 r_{\hat{s}}^{-\alpha} \frac{t_{\hat{s},\hat{s}}}{t_{\hat{s}}}}\right]\right]. \end{aligned} \tag{10}$$

By applying the probability generating functional of two-dimensional homogeneous PPP [26], [27] to (10), we have

$$\begin{aligned} &\mathcal{L}_{I_{\hat{s},\hat{s}}}(s) \\ &= \exp\left(-\rho_{\hat{s}} \int_{\mathbb{R}^2} \left(1 - \mathbb{E}_{t_{\hat{s},\hat{s}}}\left[\frac{1}{1 + sA_0 x^{-\alpha} \frac{t_{\hat{s},\hat{s}}}{t_{\hat{s}}}}\right]\right) dx\right) \\ &\overset{(c)}{=} \exp\left(-2\pi\rho_{\hat{s}} \int_0^R \left(1 - \mathbb{E}_{t_{\hat{s},\hat{s}}}\left[\frac{1}{1 + sA_0 x^{-\alpha} \frac{t_{\hat{s},\hat{s}}}{t_{\hat{s}}}}\right]\right) x dx\right) \\ &= \exp(-2\pi\rho_{\hat{s}} I_s), \end{aligned} \tag{11}$$

where $I_s = \int_0^R (1 - \mathbb{E}_{t_{\hat{s},\hat{s}}}[\frac{1}{1+sA_0 x^{-\alpha}\frac{t_{\hat{s},\hat{s}}}{t_{\hat{s}}}}])x dx$. Here, (c) follows from the transformation of Cartesian to polar coordinates. The limit of integral in (11) varies from 0 (lower limit) to R (upper limit) because the interfering EDs lies ubiquitously in a circular disc of radius R [see Fig. 2(c)]. Note that, $\rho_{\hat{s}}$ denotes the density of ED corresponding to SF $\hat{s}$, which can be calculated as follows. Suppose there are N_1 number of EDs having SNR greater than Δ_1. Hence, under the co-SF interference scenario, the interference will be experienced from these N_1 number of EDs, i.e., the total number of interferers will be $N_1 - 1$. The density of EDs assigned with SF7 is given by $\rho_1 = \frac{P_{\gamma_1} N}{\pi R^2}$. Similarly, the density of EDs assigned with SF j, where $j = \{2, \ldots, S\}$ is given by $\rho_j = \frac{P_{\gamma_j} N}{\pi R^2}$. Now the expectation term in $I_{\hat{s}}$ can be expanded as

$$\begin{aligned} &\mathbb{E}_{t_{\hat{s},\hat{s}}}\left[\frac{1}{1 + sA_0 x^{-\alpha} \frac{t_{\hat{s},\hat{s}}}{t_{\hat{s}}}}\right] \\ &= \int_{t_{\hat{s},\hat{s}}\in T_c}\left[\frac{1}{1 + sA_0 x^{-\alpha} \frac{t_{\hat{s},\hat{s}}}{t_{\hat{s}}}}\right] f_{t_{\hat{s},\hat{s}}}(t) dt_{\hat{s},\hat{s}} \end{aligned} \tag{12}$$

Solving the integration of (12), it can be expressed as follows:

$$\mathbb{E}_{t_{\hat{s},\hat{s}}}\left[\frac{1}{1+sA_0x^{-\alpha}\frac{t_{\hat{s},\hat{s}}}{t_{\hat{s}}}}\right]=\left(1-\frac{t_{\hat{s},\hat{s}}}{T_c^2}(2T_c-t_{\hat{s},\hat{s}})\right)\delta(t)+\frac{2t_{\hat{s},\hat{s}}x^{\alpha}}{s^2A_0^2T_c^2}\left[\{A_0T_cs-t_{1,1}(x^{\alpha}+A_0\,s)\}\log\left(1+sA_0x^{-\alpha}\right)\right]. \tag{13}$$

Setting $s=\frac{\delta_{\hat{s}}r^{\alpha}}{A_0}$ in (13) and substitute back the resultant expression into (11), and again substitute back the resultant expression into (8), we can obtain the expression for the first term of (4) and (5). The resulting expression is given by (14), where $\rho_{\hat{s}}=\frac{P_{\gamma_{\hat{s}}}\cdot N}{\pi R^2}$.

Now the lower bound for the PSP contributed by the EDs that are assigned SF7 can be obtained by multiplying (14) shown at bottom of this page, calculated at $\hat{s}=1$, and (6). Similarly, the lower bound for the PSP contributed by the EDs that are assigned SF j can be obtained by multiplying (14) calculated at $\hat{s}=\{2,\ldots,S\}$, and (7). In order to obtain the average PSP, we obtain the pdf of distance r between typical ED and the serving gateway. Since we assume the EDs are uniformly distributed in a circular disc of radius R, the pdf $f_R(r)$ of the distance (r) is given by [17], i.e.,

$$f_R(r)=\frac{2r}{R^2},\qquad r\leq R \tag{15}$$

Hence, the PSP of PA1 averaged over pdf $f_R(r)$ can be calculated as

$$\mathrm{PSP}_{\mathrm{PA1},av}=\sum_{\hat{s}\in\mathbb{S}}\int_0^R\mathrm{PSP}_{\mathrm{PA1}}(r,\delta_{\hat{s}})f_R(r)dr. \tag{16}$$

In the next section, we are going to introduce another algorithm for SNR-based SF allocation scheme.

Algorithm 1: SF Allocation: PA2.

Input: N = Number of EDs deployed in a circular disc
Output: PSP_{av} // `average PSP`
1: (a) Define R, P, α, T_c, f, B.
   (b) Set the location of gateway at origin.
2: (a) find the distance from gateway to each ED.
   (b) **for** $i=1$ to N **do**
      calculate $\hat{\gamma}_i$
   end for
3: Calculate the SNR threshold ($T_{\hat{s}}$) based on stochastic geometry (see eq. (19)).
4: Assign SF based on calculated SNR threshold, using the relation $T_{\hat{s}}<\frac{PA_0gr^{-\alpha}}{\sigma^2}<T_{\hat{s}-1}$.
   (a) Define SF $\hat{s}$, where $\hat{s}=\{1,2,\ldots,S\}$ define the index assigned to SF, $S=|SF|$.
5: (b) Divide the set of N EDs into S subsets of equal size: $\{\{G_1\},\{G_2\},\ldots,\{G_S\}\}$, where $\{G_{\hat{s}}\}$, $\hat{s}=\{1,2,\ldots,S\}$ denote the subset of size $\frac{N}{S}$ that contain the EDs following the relation given in step 4, i.e., $G_1=ED_1,ED_2,\ldots,ED_{N/S}$, $G_2=ED_{\frac{N}{S}+1},ED_{\frac{N}{S}+2},\ldots,ED_{\frac{2N}{S}},\cdots$, $G_S=ED_{\frac{(S-1)N}{S}+1},ED_{\frac{(S-1)N}{S}+2},\ldots,ED_N$.
6: **for** $\hat{s}=1$ to S **do**
      $G_{\hat{s}}:=$ SF $\hat{s}$
   end for
7: Calculate collision overlap time corresponding to each SF.
8: Calculate SIR corresponding to each SF.
9: Calculate average PSP.
10: **return** PSP_{av}

B. Proposed Algorithm 2 (PA2)

The proposed algorithm 2 (PA2) assigns an equal number of EDs to each SF. The motivation behind PA2 is stated as follows: in high-density scenarios, assigning SFs to EDs in an uneven fashion may increase the cochannel interference. For example, if a large number of EDs get assigned to any particular SF, the gateway will experience high cochannel interference. Hence, we propose an algorithm that assigns an equal number of EDs to each SF based on SNR. The steps involved in the PA2 are presented in Algorithm 1. The PA2 first calculate the SNR threshold ($T_{\hat{s}}$) corresponding to SF $\hat{s}$ based on the stochastic geometry. The SNR threshold is calculated such that an equal number of EDs get assigned to each SF. Then, SF is assigned based on calculated $T_{\hat{s}}$ i.e., the number of EDs for which SNR of the received packet lies between $T_{\hat{s}}<\frac{PA_0gr^{-\alpha}}{\sigma^2}<T_{\hat{s}-1}$ is assigned SF $\hat{s}$. Note that the values for $T_{\hat{s}}$ define the boundaries of each SF based on the SNR value. We now find the $T_{\hat{s}}$ of each SF for PA2, where each SF is assigned an equal number of EDs.

Calculation of SNR threshold: Since, we have considered SFs ranging from 7 to 12, i.e., $\mathbb{S}=\{1,2,\ldots,6\}$, where $|\mathbb{S}|=6$, the SNR threshold corresponding to SF $\hat{s}$ can be calculated as follows: the probability that equal number of EDs get assigned to each SF is given by

$$\mathbb{P}[\Upsilon(r)\geq T_{\hat{s}}]=\frac{\hat{s}}{6}, \tag{17}$$

where $T_{\hat{s}}$ denotes the SNR threshold corresponding to SF $\hat{s}$. Substituting the expression for $\Upsilon(r)$ in (17), and following the fact that $g\sim\exp(1)$, (17) can be expressed as

$$\exp\left(-\frac{\sigma^2T_{\hat{s}}r^{\alpha}}{PA_0}\right)=\frac{\hat{s}}{6}. \tag{18}$$

$$\mathbb{P}[\eta_{\hat{s}}(r)>\delta_{\hat{s}}]=\exp\left\{-2\pi\rho_{\hat{s}}\int_0^R\left[1-\left\{\left(1-\frac{t_{\hat{s},\hat{s}}}{T_c^2}(2T_c-t_{\hat{s},\hat{s}})\right)\delta(t)+\frac{2t_{\hat{s},\hat{s}}x^{\alpha}}{\delta_{\hat{s}}^2r^{2\alpha}T_c^2}\left[\{T_c\delta_{\hat{s}}r^{\alpha}-t_{\hat{s},\hat{s}}(x^{\alpha}+\delta_{\hat{s}}r^{\alpha})\}\log\left(1+\delta_{\hat{s}}\left(\frac{r}{x}\right)^{\alpha}\right)\right]\right\}\right]xdx\right\} \tag{14}$$

Hence, the SNR threshold corresponding to SF $\hat{s}$ is given by

$$T_{\hat{s}} = -\frac{\ln(\frac{\hat{s}}{6})PA_0 r^{-\alpha}}{\sigma^2}. \tag{19}$$

In the next section, we will obtain the expression of the PSP for PA2 using the calculated SNR threshold.

C. PSP: PA2

In PA2, a packet having SF $\hat{s}$ can successfully communicate with the gateway if it satisfies the following three conditions: (i) the SNR of the received packet is greater than SF specific SNR threshold ($T_{\hat{s}}$) but less than $T_{\hat{s}-1}$, that is, $T_{\hat{s}} < \frac{PA_0 gr^{-\alpha}}{\sigma^2} < T_{\hat{s}-1}$, (ii) the SNR of the received packet is greater than SF specific target SNR ($\Delta_{\hat{s}}$), that is, $\frac{PA_0 gr^{-\alpha}}{\sigma^2} > \Delta_{\hat{s}}$, and (iii) the SIR ($\eta_{\hat{s}}$) of the received packet is greater than the SF specific SIR threshold ($\delta_{\hat{s}}$), that is, $\frac{A_0 gr^{-\alpha}}{I_{\hat{s}}} > \delta_{\hat{s}}$. The PSP contributed by the EDs that are assigned an SF7 can be defined as follows:

$$\begin{aligned}\text{PSP}_{\text{PA2}}(r,\delta_1) &= \mathbb{P}\left[\{\eta_1(r) > \delta_1\} \bigcap \{\Upsilon(r) > \max(T_1,\Delta_1)\}\right] \\ &\geq \mathbb{P}\left[\eta_1(r) > \delta_1\right] \mathbb{P}\left[\Upsilon(r) > \max(T_1,\Delta_1)\right].\end{aligned} \tag{20}$$

Similarly, the PSP contributed by the EDs operating at SF j, where $j \in \{2,\ldots,S\}$ can be defined as

$$\begin{aligned}&\text{PSP}_{\text{PA2}}(r,\delta_j) \\ &= \mathbb{P}\left[\{\eta_j(r) > \delta_j\} \bigcap \{\max(T_j,\Delta_j) < \Upsilon(r) < T_{j-1}\}\right] \\ &\geq \mathbb{P}\left[\eta_j(r) > \delta_j\right] \mathbb{P}\left[\max(T_j,\Delta_j) < \Upsilon(r) < T_{j-1}\right].\end{aligned} \tag{21}$$

The second term in (21) holds for the condition $T_{j-1} > \max(T_j,\Delta_j)$. The first term in (20) and (21) can be obtained from (14) by setting $\hat{s}=1$, except for the fact that the density of EDs in PA2 is different, which is given by $\rho_{\hat{s}} = \frac{\rho}{6}$. Now we obtain the expression for the second term in (20), that is, $\mathbb{P}[\Upsilon(r) > \max(T_1,\Delta_1)]$, which can be expanded as

$$\begin{aligned}\mathbb{P}[\Upsilon(r) > \max(T_1,\Delta_1)] &= \mathbb{P}\left[g > \frac{\max(T_1,\Delta_1)\sigma^2 r^\alpha}{PA_0}\right] \\ &\overset{(d)}{=} \exp\left(-\frac{\max(T_1,\Delta_1)\sigma^2 r^\alpha}{PA_0}\right).\end{aligned} \tag{22}$$

Here, (d) follows from the assumption $g \sim \exp(1)$. The second term in (21), i.e., $\mathbb{P}\left[\max(T_j,\Delta_j) < \Upsilon(r) < T_{j-1}\right]$ (let it be denoted by $\hat{P}_{\Upsilon_j}$) can be determined by following the same steps as in (7). The final expression for $\hat{P}_{\Upsilon_j}$ is given as,

$$\begin{aligned}\hat{P}_{\Upsilon_j} &= \exp\left(-\frac{\max(T_j,\Delta_j)\sigma^2 r^\alpha}{PA_0}\right) - \exp\left(-\frac{T_{j-1}\sigma^2 r^\alpha}{PA_0}\right) \\ &j = \{2,\ldots,S\}.\end{aligned} \tag{23}$$

Now the lower bound for the PSP contributed by the EDs that are assigned SF7 can be obtained by multiplying (14) calculated at $\hat{s}=1$, $\rho_{\hat{s}} = \frac{\rho}{6}$ and (22). Similarly, the lower bound for the PSP contributed by the EDs that are assigned SF j, where $j \in \{2,\ldots,S\}$ can be obtained by multiplying (14) calculated at $\hat{s} = \{2,\ldots,S\}$, $\rho_{\hat{s}} = \frac{\rho}{6}$, and (23). Hence, the PSP averaged over pdf $f_R(r)$ for PA2 is given by

$$\text{PSP}_{\text{PA2},av} = \sum_{\hat{s}\in\mathbb{S}} \int_0^R \text{PSP}_{\text{PA2}}(r,\delta_{\hat{s}}) f_R(r) dr. \tag{24}$$

TABLE II
SIMULATION PARAMETERS

Parameters	Value
Carrier frequency (f)	867 MHz
Transmit power of each ED (P)	14 dBm
Bandwidth (B)	125 KHz
Path-loss exponent (α) [17]	3
Contention time period (T_c)	60 sec

VI. RESULTS AND DISCUSSION

In this section, we present the numerical results to analyze the scalability of LoRaWAN for the proposed SF allocation scheme. We performed Monte-Carlo simulations in MATLAB to obtain the results. Note that all our results are based on Rayleigh fading. The EDs are distributed in a circular disc of radius R according to PPP, where the value of R is considered in the range $[10-30]$ km [17], [21]. While the exact value of R is specified with the plot itself. The LoRa gateway is assumed to be located at the center of the disc. To calculate the PSP of the desired uplink transmission at the gateway, we performed the following steps. First, we obtained the received SNR for each ED at the gateway. Then, based on the proposed schemes: PA1 or PA2, we allocate SF to each ED. The PSP for PA2 is calculated based on three conditions: (i) the SNR of the received packet is greater than the SF specific SNR threshold given in Table I, (ii) the SNR of the received packet is greater than SF specific target SNR, and (iii) the SIR of the received packet is greater than the SF specific SIR threshold. On the other hand, the PSP for PA1 is calculated based on two conditions: (i) the SNR of the received packet is greater than the SF specific SNR threshold but less than the SNR threshold corresponding to the next higher SF, (ii) the SIR of the received packet is greater than the SF specific SIR threshold. The parameters with their values used for obtaining the results are listed in Table II.

A. Comparison of Different SF Allocation Schemes

Fig. 3 compares the PSP of proposed schemes (PA1 and PA2) with existing EIB and EAB schemes[3] for two different values of radius: $R = 20$ km in Fig. 3(a) and $R = 30$ km in Fig. 3(b). The EIB and EAB schemes are introduced below.

1) EIB scheme: The circular disc is divided into S concentric circles such that the width of each annulus is same. The EIB scheme determines the width of annulus (w_i), according to $w_i = \frac{R}{S}$.
2) EAB scheme: The circular disc area is divided into S areas such that each annulus gets an equal area. The EAB

[3]where, the results plotted for EIB and EAB schemes are obtained from the article [17].

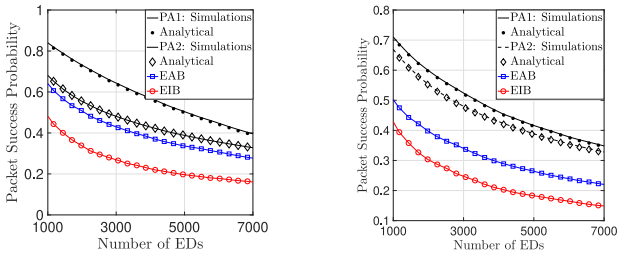

Fig. 3. PSP comparison of proposed algorithms (PA1 and PA2) with EIB and EAB SF allocation scheme for two different values of radius. Here, packet size of 10 bytes is considered. (a) $R = 20$ km. (b) $R = 30$ km.

TABLE III
PARAMETERS FOR SF ALLOCATION SCHEMES

Parameters	EIB	EAB
Width	$w_i = \frac{R}{S}$	$w_i = l_i - l_{i-1}$ $l_i = R\sqrt{\frac{i}{S}}$
Area	$A_i = \pi w_i^2(2i-1)$	$A_i = \frac{\pi R^2}{S}$

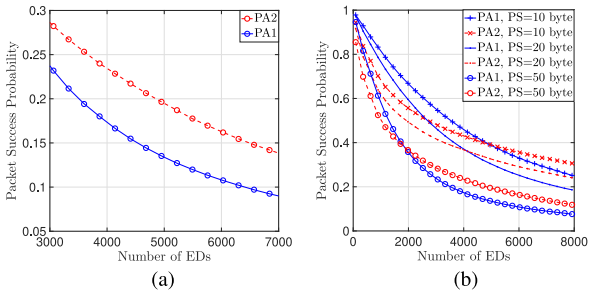

Fig. 4. PSP versus N for different packet sizes. (a) $R = 10$ km, $PS = 50$ bytes. (b) $R = 10$ km.

scheme determines the width of annulus, according to $w_i = R\sqrt{\frac{i}{S}}$ [17].

The annuli parameters for EIB and EAB SF allocation schemes are defined in Table III . While the values of all other parameters are given in Table II. In these results, a packet size of 10 b is considered for computing the PSP. From these results, the following two important observations can be made. First, the proposed scheme performs better than both EIB and EAB schemes in terms of LoRa scalability. Note that since the proposed schemes allocate SF based on the instantaneous SNR, it takes advantage of the fact that the lower SF possesses lower receiver sensitivity, while the higher SF possesses higher receiver sensitivity. Therefore, assigning lower SF to EDs having the lowest SNR value while assigning higher SF to EDs having higher SNR value improves the PSP. Second, PA1 has a higher PSP compared to PA2. However, a similar plot for high-density scenario and large packet size [Fig. 4(a)] showed that PA2 has a higher PSP in comparison to PA1. This is because, in PA1, the impact of packet collision becomes more dominant with the increasing packet sizes and ED densities.

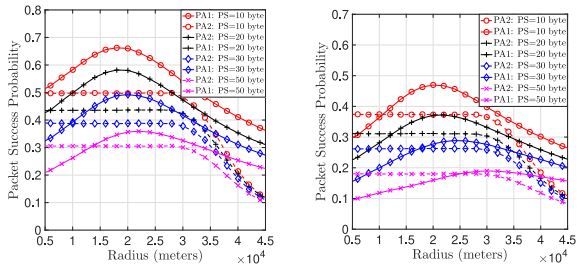

Fig. 5. PSP variation with respect to R for different packet size. (a) $N = 2700$. (b) $N = 5400$.

B. Effects of LoRa Packet Size on PSP

In the LoRa network, different packet sizes lead to different packet duration [28]. Moreover, for fixed packet size, packet duration also varies with SF (as depicted in Table I).

Fig. 4(b) plots the PSP of proposed schemes (PA1 and PA2) for different packet sizes (10 , 20 , and 50 b). It can be observed that the PSP decreases with the increase in packet size. It is because the packet duration increases with an increase in the packet size. Hence, the effect of packet collision becomes more dominant with the increase in packet sizes. Moreover, it can be observed that for fixed packet size and low ED density, PA1 has a higher PSP than PA2. Furthermore, note that with the increase in ED density, the PSP of PA1 decreases more than the PSP of PA2. This is because, in PA1, a larger fraction of ED density gets assigned to any single SF. Therefore, compared to PA2, the packet collision probability for PA1 is significantly higher. Consequently, after a specific ED density, the PSP of PA2 exceeds PA1. Furthermore, it can be observed that, with the increase in packet size, the PSP of PA2 starts exceeding that of PA1 at comparatively lower ED densities. This is because of the dominating effect of a collision.

C. Effects of Cell Radius on PSP

Fig. 5 shows the variation of PSP with respect to R for different packet sizes. Two different plots for $N = 2700$, and $N = 5400$ are shown. The following observations can be made from these plots.

1) For PA1, the PSP first increases with the increase in R. This is because, at smaller cell sizes, a larger number of EDs are present in the lower SF. However, as R increases, some EDs shift from lower SF to higher SF. Therefore, the packet collision decreases, and as a result, the PSP increases. Although, after a certain R, PSP decreases with the increase in R because the number of EDs that satisfy condition-(i) (i.e., the SNR of the received packet is greater than the SF specific SNR threshold) decreases.
2) In PA2, an equal number of EDs are assigned to each SF. Therefore, the PSP remains almost constant up to $R = 28$ km (according to Fig. 5). Subsequently, increasing the R reduces the PSP, because the number of EDs satisfying the condition-(i) decreases.
3) Apart from this, it can be seen that the PSP of PA2 is higher than the PSP of PA1 at high ED density (which is

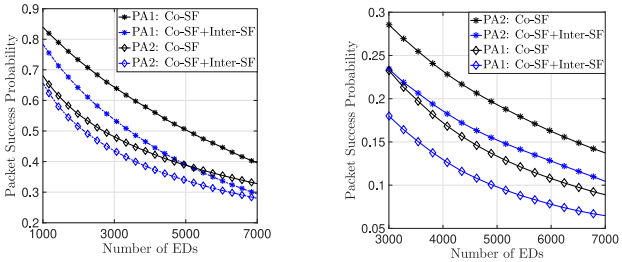

Fig. 6. PSP comparison of PA1 and PA2 under co-SF and co-SF + inter-SF interference. (a) $R = 20$ km and PS $= 10$ bytes. (b) High-density scenario: $R = 10$ km and PS$= 50$ bytes.

analogous to a small radius for a fixed number of EDs) for large packet size. This is because, in the high-density scenario, PA1 allocates a large number of EDs to lower SFs, whereas PA2 allocates an equal number of EDs to each SF. As a result, the impact of cochannel interference becomes more dominant for PA1. The impact is significant for larger packet sizes, where the chances of collision are more.

4) Also, it can be seen that, for higher N, the PSP of PA2 is higher than the PSP of PA1 over wide range of R.

D. Impact of Inter-SF Interference on PSP

In the case of imperfect orthogonality among the nodes operating in different annulus regions, the performance of the LoRa network may also be influenced by inter-SF interference, along with co-SF interference. Let μ_{ij} denotes the target SIR for successful packet reception of a packet sent at SF_i (desired signal) under the concurrent transmission of packet at SF_j (interfering signal). The packet transmitted at SF_i under the concurrent transmission of packet SF_j can be successfully received, if the SIR of the desired signal is abovementioned the μ_{ij}. The values of μ_{ij} for $i, j = \{7, 8, \ldots, 12\}$ are given by target SIR matrix Λ(dB) [17].

$$\Lambda(\text{dB}) = \begin{array}{c} \\ SF_7 \\ SF_8 \\ SF_9 \\ SF_{10} \\ SF_{11} \\ SF_{12} \end{array} \begin{array}{c} \begin{array}{cccccc} SF_7 & SF_8 & SF_9 & SF_{10} & SF_{11} & SF_{12} \end{array} \\ \begin{pmatrix} 1 & -8 & -9 & -9 & -9 & -9 \\ -11 & 1 & -11 & -12 & -13 & -13 \\ -15 & -13 & 1 & -13 & -14 & -15 \\ -19 & -18 & -17 & 1 & -17 & -18 \\ -22 & -22 & -21 & -20 & 1 & -20 \\ -25 & -25 & -25 & -24 & -23 & 1 \end{pmatrix} \end{array}. \quad (25)$$

Each element in Λ(dB) gives the value of μ_{ij}. Note that, for $i = j$, the matrix elements in (25) defines the target SIR for co-SF interference scenario. While for $i \neq j$, the matrix elements in (25) defines the target SIR for inter-SF interference scenario. Fig. 6 shows the impact of inter-SF interference along with co-SF interference on PSP for PA1 and PA2, respectively. The parameter values (i.e., R and packet size) used to obtain the results are given in the caption of each figure. The following useful insights can be drawn from the plots shown in Fig. 6.

1) It can be seen that PSP performance is mainly affected by co-SF interference [Fig. 6(a) and (b)].
2) However, due to incomplete orthogonality, inter-SF interference causes a further drop in PSP. Note that the drop in PSP due to inter-SF interference increases with the increase in the number of concurrently transmitting EDs [Fig. 6(a)]. This is because, with the increase in the number of concurrently transmitting EDs, the number of transmitting EDs satisfying the target SIR condition of inter-SF interference [defined by the elements of the matrix given in (25)] decreases.
3) The loss in PSP due to inter-SF interference is more for PA1 than PA2 [Fig. 6(a)]. The reason is as follows: In PA1, different SFs are assigned an unequal number of EDs. Typically, in PA1, a relatively large number of EDs are assigned to the lower SF. Hence, a lesser number of EDs from higher SFs satisfied the target SIR condition [target SIR matrix (25)] with respect to the interfering transmissions from lower SF annulus.
4) PA1 has a higher PSP than PA2 for both the co-SF and co-SF + inter-SF interference scenario.
5) Moreover, a similar plot for the high-density scenario and for larger packet size [Fig. 6(b)] shows that PA2 has higher PSP than PA1 under both the co-SF interference scenario and the co-SF + inter-SF interference scenario.

E. Remarks: Selection of PA1 and PA2

It can be observed that both PA1 and PA2 outperform the conventional EIB and EAB schemes in terms of PSP. However, neither of them is consistently better than the other. Hence, the question arises, which of these two schemes should be used in different scenarios. We provide the following remarks that could help this choice.

1) Based on the ED density and packet size, PA1 or PA2 can be selected: In a low ED density scenario, PA1 should be used. However, in a high ED density scenario, PA2 should be used. The reason is, at low ED density, the impact of cochannel interference is less.
2) For a small packet size, PA1 should be used; however, for a large packet size, PA2 should be used. The reason being packet duration increases with an increase in packet size. In other words, the impact of interference due to packet collision becomes more dominant with the increase in packet size. The impact is even more dominant when a higher portion of the ED density gets assigned to a single SF. Hence, PA2 should be used for a larger packet size.
3) From the discussion, it is concluded that PSP performance is mainly affected by co-SF interference. Therefore, the inclusion of inter-SF interference does not violate the choice of PA1 and PA2.

VII. Hardware Design and Implementation of Proposed Work in Real-Life Scenarios

This section gives an overview of hardware components used in the LoRa systems. Also, this section describes how the proposed work can be implemented in real scenarios and lists some real-life applications that can be solved.

(a) (b)

Fig. 7. Hardware components of LoRaWAN. (a) End-device. (b) Gateway.

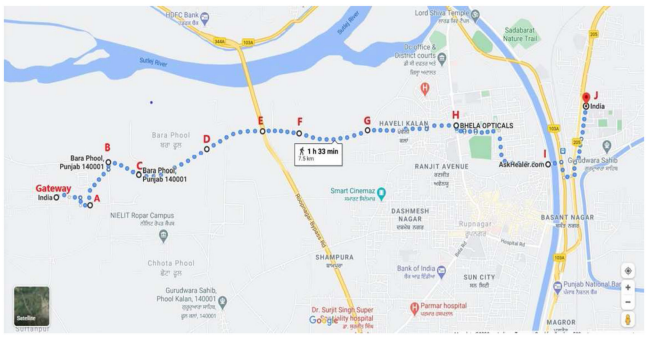

Fig. 8. Considered path between IIT Ropar main-campus and IIT Ropar transit-campus for the measurement of SNR at different places, which is shown by map created from Google maps [29]. Here, the markers (labeled from A to J) indicate the measurement points.

A. Hardware Design

The hardware of the LoRa system includes EDs and gateway. We have EDs in our lab using RFM95 W LoRa module [shown in Fig. 7(a)]. Its major components are listed below.

1) MCU-Atmega328P-AU: It is an 8-b microcontroller by Atmel. Microcontroller is connected to the LoRa Module via serial peripheral interface.
2) LoRa Module (RFM95 W): It is based on Semtech Sx1276 LoRa transceiver. It transmits the data received from the sensor to gateway.
3) Antenna: ED is equipped with an external dipole antenna. The external dipole antenna has the following features: operating frequency- 860 − 880 MHz, radiation- omni-directional, antenna gain- 2 dBi.

On the other hand, we have considered a RAK7258 gateway by RAK wireless [shown in Fig. 7(b)].

B. Experiment Setup and Implementation in Real Scenarios

We have performed real-time experiments and have shown SNR variations up to 5.9 km distance. The experiment is performed in an urban environment. In particular, we have considered the place between the IIT Ropar main-campus and IIT Ropar transit-campus (shown in Fig. 8), which is about a 5.9 km distance via a direct path. The experimental setup of the LoRa system for its real-time implementation is shown in Fig. 9. The gateway station is installed on the second floor of the building at our campus. In the experiments, LoRa ED continuously sends uplink packets and gradually moves away from the location

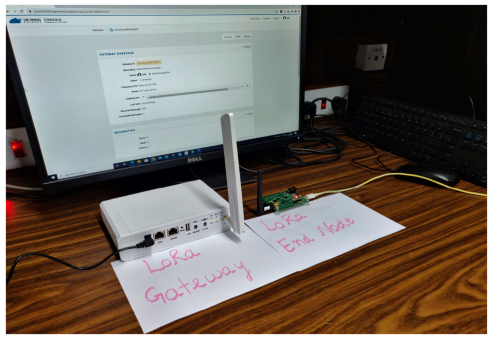

Fig. 9. Experimental setup for implementation in real scenarios.

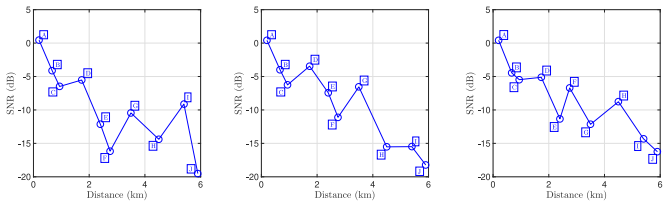

(a) (b) (c)

Fig. 10. SNR variations with distance for three different days. (a) Day-1. (b) Day-2. (c) Day-3.

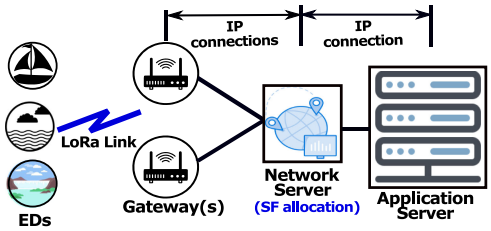

Fig. 11. LoRaWAN architecture: Compatibility with proposed work.

of the LoRa gateway. The experiment is performed on three different days, and SNR is measured over several points marked in Fig. 8 (i.e., points A to J). The variations of SNR at these selected points are shown by plots in Fig. 10. It can be seen that the SNR is fluctuating with distance. Then, based on these SNR variations, one can implement our algorithms on the network server. Based on our proposal, we have highlighted the required changes in the blocks of the LoRaWAN system. Where the LoRaWAN architecture is shown in Fig. 11. While the role of each block is defined below.

1) ED: EDs transmit packets to gateway via LoRa link.
2) Gateway: Functions as a relay between EDs and network server, i.e., it simply forwards the packets from/to EDs to/from network server via internet.
3) Network server: Manages the entire network, i.e., it is responsible for resource allocation (i.e., SF and bandwidth), handles the deduplication of received packets.
4) Application server: Interpreted and displays the data received from the network server.

The proposed method can be implemented as follows. EDs send their packets to the gateway with uplink channel information. LoRa gateway then forwards all uplink radio packets to the LoRa network server after adding metadata such as SNR.

TABLE IV
LoRaWAN Attack Types, With Their Description, Implication on System Performance, and Possible Solutions [30]–[35]

Attack Type	Attack Description	Implication on System Performance	Possible Solutions
Jamming Attack	Jammer continuously transmits a radio frequency signal at the same frequency as the ongoing radio transmission between ED and gateway.	Cut-off the ongoing communication between ED and gateway, increase in congestion.	Switching to another frequency.
Collision Attack	The attacker transmits the packet at the same time and the frequency at which the valid packet transmission takes place.	Increases collision.	LoRaWAN can adopt different frequency hopping and spread spectrum techniques to increase the uncertainty for an attacker.
Replay Attack	The hacker detects a valid packet transmission and then resend it to the receiver.	Duplication of packets, increase congestion.	Periodically change the servers access keys (i.e., network and application servers keys), use timestamps with the messages.

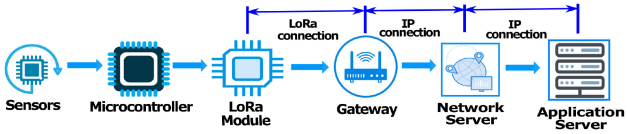

Fig. 12. Typical setup (in sequence of data flow) for real-time implementation of proposed work.

The network server regularly runs the proposed algorithm and accordingly allocates SF to each ED. The SF allocation is updated with the instantaneous channel report. The data is then sent to the application server via the internet, which interprets and displays the received data.

C. Applications of Proposed Work

The proposed work is suitable for a wide range of telemetry applications (i.e., sensing and monitoring). These applications mainly include long-range communications in inaccessible areas (sea-to-ground communication, real-time water quality monitoring, monitoring activities within the marine environment), smart city applications (air-quality monitoring, waste management), smart agriculture applications (temperature, water level, moisture monitoring), and industrial IoT applications (item location and tracking).

A typical setup for real-time implementation of these applications, according to the data flow (i.e., from sensing to processing, remotely transmitting, and displaying data), is shown in Fig. 12. The data sensing is performed prior to LoRa transmission, which includes modules such as application-specific sensor, a microcontroller, and a LoRa transceiver module. Depending on the applications, various sensors are used to collect data from the surrounding environment or object. The data pin of the sensor is then interfaced with the microcontroller pin, which receives sensor readings and passes it to the LoRa transceiver module (e.g., RFM95 W module). The RFM95 W LoRa transceiver module communicates with the LoRa gateway via the LoRa link. The gateway then forwards the information received from EDs to the network server via an internet connection. The data is then sent to the application server via the internet, which interprets and displays the received data.

D. LoRaWAN Security

LoRaWAN may suffer from some security issues. These security issues include different types of attacks, such as the jamming attack, collision attack, replay attack, etc. However, the presented work can be protected from these attacks if some security measures are followed. The various LoRaWAN attack types, their implication on system performance, and possible solutions to protect against these attacks can be found in [30]–[35]. They are summarized in Table IV.

Besides, it is also important to constantly monitor LoRaWAN networks for detecting and preventing attacks. The vendor default keys should be replaced with random and different keys for each ED. Also, secure elements and hardware security modules should be used so that the keys are never disclosed. Finally, all LoRaWAN infrastructure must be security audited time-to-time to identify and fix security issues.

VIII. Conclusion

In this article, we proposed an SNR-based SF allocation scheme. In particular, we proposed two algorithms based on the proposed scheme. Using the stochastic-geometry, PSP expressions were derived for both the algorithms, and they were compared with state-of-art EIB and EAB SF allocation schemes. The obtained results showed that the proposed algorithms outperform both EIB and EAB SF allocation schemes. Furthermore, the proposed algorithms were compared to each other. Where the comparison showed that both algorithms outperform each other in different scenarios. Therefore, remarks were given to select PA1 and PA2 in different scenarios. It is concluded that PA1 outperforms PA2 in low ED density and large packet size scenarios. While PA2 outperforms PA1 in the case of high ED density and smaller packet sizes. Also, we analyzed the impact of various parameters viz. radius and packet size on the PSP. Finally, we proved the applicability of the presented work in real-life scenarios by performing real-time experiments.

References

[1] U. Raza, P. Kulkarni, and M. Sooriyabandara, "Low power wide area networks: An overview," *IEEE Commun. Surv. Tut.*, vol. 19, no. 2, pp. 855–873, Apr./Jun. 2017.
[2] Link-Labs, "A comprehensive look at low power wide area networks for Internet of Things engineers and decision makers," Dec. 2016. [Online]. Available: https://www.linklabs.com/symphony
[3] A. Lavric, A. I. Petrariu, and V. Popa, "Long range sigfox communication protocol scalability analysis under large-scale, high-density conditions," *IEEE Access*, vol. 7, pp. 35 816–35 825, 2019.
[4] Y. E. Wang *et al.*, "A primer on 3GPP narrowband Internet of Things," *IEEE Commun. Mag.*, vol. 55, no. 3, pp. 117–123, Mar. 2017.
[5] A. Ikpehai *et al.*, "Low-power wide area network technologies for Internet-of-Things: A comparative review," *IEEE Internet Things J.*, vol. 6, no. 2, pp. 2225–2240, Apr. 2019.
[6] J. P. S. Sundaram, W. Du, and Z. Zhao, "A survey on LoRa networking: Research problems, current solutions and open issues," *IEEE Commun. Surv. Tut.*, vol. 22, no. 1, pp. 371–388, Jan.–Mar. 2020.

[7] L. Vangelista, "Frequency shift chirp modulation: The LoRa modulation," *IEEE Signal Process. Lett.*, vol. 24, no. 12, pp. 1818–1821, Dec. 2017.
[8] Semtech, "LoRa Modulation Basics, AN1200. 22, Revision 2," 2015.
[9] F. Adelantado, X. Vilajosana, P. Tuset-Peiro, B. Martinez, J. Melia-Segui, and T. Watteyne, "Understanding the limits of LoRaWAN," *IEEE Commun. Mag.*, vol. 55, no. 9, pp. 34–40, Sep. 2017.
[10] L. D. Xu, W. He, and S. Li, "Internet of Things in industries: A survey," *IEEE Trans. Ind. Informat.*, vol. 10, no. 4, pp. 2233–2243, Nov. 2014.
[11] E. Sisinni *et al.*, "A LoRaWAN range extender for industrial IoT," *IEEE Trans. Ind. Informat.*, vol. 16, no. 8, pp. 5607–5616, Aug. 2020.
[12] J. Markkula, K. Mikhaylov, and J. Haapola, "Simulating LoRaWAN: On importance of inter spreading factor interference and collision effect," in *Proc. IEEE Int. Conf. Commun.*, May 2019, pp. 1–7.
[13] K. Mikhaylov and T. Haenninen, "Analysis of capacity and scalability of the LoRa low power wide area network technology," in *Proc. 22nd Eur. Wireless Conf.*, May 2016, pp. 1–6.
[14] O. Georgiou and U. Raza, "Low power wide area network analysis: Can LoRa scale?," *IEEE Wireless Commun. Lett.*, vol. 6, no. 2, pp. 162–165, Apr. 2017.
[15] F. Van den Abeele, J. Haxhibeqiri, I. Moerman, and J. Hoebeke, "Scalability analysis of large-scale LoRaWAN networks in NS-3," *IEEE Internet Things J.*, vol. 4, no. 6, pp. 2186–2198, Dec. 2017.
[16] R. B. Sorensen, N. Razmi, J. J. Nielsen, and P. Popovski, "Analysis of LoRaWAN uplink with multiple demodulating paths and capture effect," in *Proc. IEEE Int. Conf. Commun.*, May 2019, pp. 1–6.
[17] A. Mahmood, E. Sisinni, L. Guntupalli, R. Rondòn, S. A. Hassan, and M. Gidlund, "Scalability Analysis of a LoRa network under imperfect orthogonality," *IEEE Trans. Ind. Informat.*, vol. 15, no. 3, pp. 1425–1436, Mar. 2019.
[18] J. M. de Souza Sant Ana, A. S. Hoeller, R. D. Souza, S. Montejo-Sanchez, H. Alves, and M. de Noronha Neto, "Hybrid coded replication in LoRa networks," *IEEE Trans. Ind. Informat.*, vol. 16, no. 8, pp. 5577–5585, Aug. 2020.
[19] A. Hoeller, R. D. Souza, O. L. Alcaraz Lòpez, H. Alves, M. de Noronha Neto, and G. Brante, "Analysis and performance optimization of LoRa networks with time and antenna diversity," *IEEE Access*, vol. 6, pp. 32 820–32 829, 2018.
[20] F. Cuomo, M. Campo, A. Caponi, G. Bianchi, G. Rossini, and P. Pisani, "EXPLoRa: Extending the performance of LoRa by suitable spreading factor allocations," in *Proc. IEEE 13th Int. Conf. Wireless Mobile Comput., Netw. Commun.*, Oct. 2017, pp. 1–8.
[21] J. Lim and Y. Han, "Spreading factor allocation for massive connectivity in LoRa systems," *IEEE Commun. Lett.*, vol. 22, no. 4, pp. 800–803, Apr. 2018.
[22] A. Waret, M. Kaneko, A. Guitton, and N. El Rachkidy, "LoRa throughput analysis with imperfect spreading factor orthogonality," *IEEE Wireless Commun. Lett.*, vol. 8, no. 2, pp. 408–411, Apr. 2019.
[23] M. A. Ullah *et al.*, "K-means spreading factor allocation for large-scale LoRa networks," *Sensors*, vol. 19, no. 21, 2019, Art. no. 4723.
[24] X. Liu, Z. Qin, Y. Gao, and J. A. McCann, "Resource allocation in wireless powered IoT networks," *IEEE Internet Things J.*, vol. 6, no. 3, pp. 4935–4945, Jun. 2019.
[25] J. Lyu, D. Yu, and L. Fu, "Achieving max–min throughput in LoRa networks," in *IEEE Int. Conf. Comput., Netw. Commun. (ICNC)*, Big Island, HI, USA, 2020, pp. 471–476.
[26] M. Haenggi, *Stochastic Geometry for Wireless Networks*. Cambridge, U.K.: Cambridge Univ. Press, 2012.
[27] D. Stoyan, W. Kendall, and J. Mecke, *Stochastic Geometry and its Applications* (Wiley Series in Probability and Mathematical Statistics: Applied Probability and Statistics). New York, NY, USA: Wiley, 1987.
[28] Semtech SX1272/3/6/7/8, "LoRa modem design guide, AN1200.13," Revision 1, 2013.
[29] "Google Maps," Accessed: Oct. 10, 2020. [Online]. Available: https://www.google.com/maps
[30] H. Noura, T. Hatoum, O. Salman, J.-P. Yaacoub, and A. Chehab, "LoRaWAN security survey: Issues, threats and possible mitigation techniques," *Internet Things*, vol. 12, 2020, Art. no. 100303.
[31] A. S. Sohal, R. Sandhu, S. K. Sood, and V. Chang, "A cybersecurity framework to identify malicious edge device in fog computing and cloud-of-things environments," *Comput. Secur.*, vol. 74, pp. 340–354, 2018.
[32] M. Ingham, J. Marchang, and D. Bhowmik, "IoT security vulnerabilities and predictive signal jamming attack analysis in LoRaWAN," *IET Inf. Secur.*, vol. 14, no. 4, pp. 368–379, 2020.
[33] W. Xu, S. Jha, and W. Hu, "LoRa-key: Secure key generation system for LoRa-based network," *IEEE Internet Things J.*, vol. 6, no. 4, pp. 6404–6416, Aug. 2019.
[34] G. K. Kurt, Y. Khosroshahi, E. Ozdemir, N. Tavakkoli, and O. A. Topal, "A hybrid key generation and a verification scheme," *IEEE Trans. Ind. Informat.*, vol. 16, no. 1, pp. 703–714, Jan. 2020.
[35] D. Basu, T. Gu, and P. Mohapatra, "Security issues of low power wide area networks in the context of LoRa networks," 2020, *arXiv:2006.16554*.